J. Fluid Mech. (2000), *vol.* 424, *pp.* 197–216. Printed in the United Kingdom

A theoretical model of a turbulent fountain

By LYNN J. BLOOMFIELD AND ROSS C. KERR

Research School of Earth Sciences, The Australian National University, Canberra, ACT 0200, Australia

(Received 28 August 1999 and in revised form 1 June 2000)

A theoretical model of axisymmetric turbulent fountains in both homogeneous and stratified fluids is developed. The model quantifies the entrainment of ambient fluid into the initial fountain upflow, and the entrainment of fluid from both the upflow and environment into the subsequently formed downflow. Four different variations of the model are considered, comprising the two most reasonable formulations of the body forces acting on the 'double' structure and two formulations of the rate of entrainment between the flows. The four model variations are tested by comparing the predictions from each of them with experimental measurements of fountains in homogeneous and stratified fluids.

1. Introduction

Turbulent fountains are formed when a continuous jet of dense fluid is injected rapidly upwards into a lighter environment (Turner 1966). The entrainment of surrounding fluid into this turbulent flow has two effects. The volume flux increases with height, while the addition of lighter ambient fluid decreases the density of the rising fluid. The velocity of the heavy upflow decreases until it falls to zero at some initial height. At this point, the flow reverses direction to fall as an annular plume which surrounds the central upflow (figure 1). The turbulent interaction between the upflow and downflow reduces the top of the fountain to a final height, which fluctuates randomly about a mean value.

Turbulent fountains arise in numerous situations – some examples which have aroused interest include: the forced heating or cooling of large structures such as aircraft hangers (Baines, Turner & Campbell 1990), the replenishment of magma chambers in the Earth's crust (Turner & Campbell 1986; Campbell & Turner 1989), the disposal of effluent into the ocean (Koh & Brooks 1975) and the exit snow from snowploughs (Lindberg & Petersen 1991). In an attempt to understand fountain behaviour under various environmental conditions, there have been a number of experimental studies in both homogeneous (Turner 1966; Seban, Behnia & Abreu 1978; Mizushina *et al.* 1982) and linearly stratified (Bloomfield & Kerr 1998) environments. In these studies, experimental measurements have been combined with dimensional analysis to determine how the fountain heights depend on the initial fluid velocity, the density difference between the source and ambient fluids, and the ambient density gradient. However, no such information exists to quantify fountain heights in an arbitrary density gradient. This is of particular importance in studies of fountains in a confined environment, where it has been shown that an initially homogeneous or linearly stratified density profile evolves with time (Baines *et al.* 1990; Bloomfield & Kerr 1999). This evolution depends sensitively on the height of the fountain, which in turn is dependent on the changing ambient density profile. In the 'fountain filling

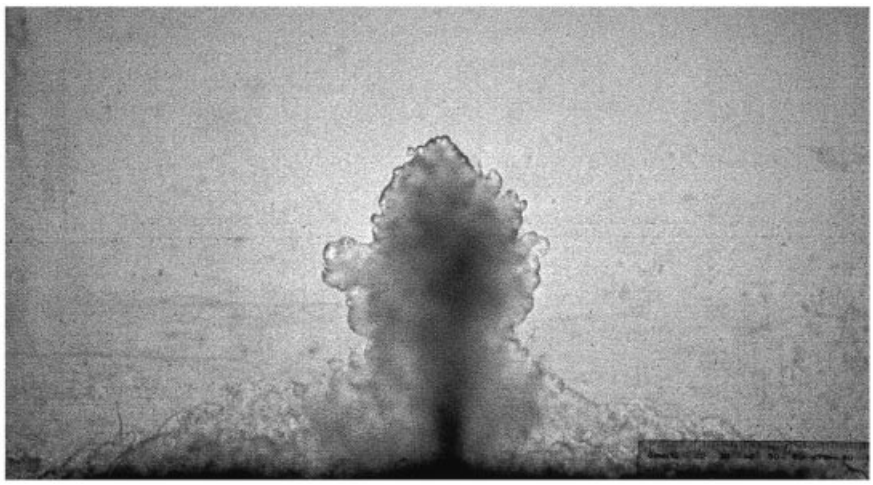

FIGURE 1. Photograph of a turbulent fountain in a homogeneous fluid.

box' models developed to date, the rate at which the fountain height increases has been found by crude interpolations from the known behaviour in homogeneous and stratified environments (Baines *et al.* 1990; Bloomfield & Kerr 1999). In this paper, we aim to develop a theoretical model that can predict the height of a turbulent fountain in an arbitrary density gradient.

In previous studies (Morton 1959; Bloomfield & Kerr 1998), the entrainment equations (Morton, Taylor & Turner 1956) have been used successfully to obtain a theoretical prediction of the initial height the fountain reaches, before the downflow has formed. However, these entrainment equations can no longer be applied once the downflow begins to interact with the upflow. To overcome this, Turner (1966) proposed that it should be possible to set up a detailed theory of the 'double' structure of the fountain in the manner suggested by Morton (1962) for coaxial turbulent jets. In that study, Morton noted that it is not immediately obvious how the simple ideas of entrainment across a jet boundary should be extended to the more complicated double structure of coaxial turbulent jets. Despite this, he proposed one formulation to quantify the mixing between the core jet and the outer, annular jet.

Morton's (1962) ideas about the rate of entrainment between two turbulent flows were subsequently used by McDougall (1981) to develop a theoretical model of an axisymmetric fountain in a homogeneous fluid. This model was based on a set of new entrainment equations which quantified the mixing between the upflow and the downflow, and between the downflow and the environment. In addition to the effects of mixing between the flows, McDougall (1981) also recognized that the body forces acting on the fluid in the upflow and downflow are 'very much an open question'. In an attempt to address this question, McDougall (1981) considered the two most reasonable formulations of the body forces acting on the fountain. From the resulting equations he was able to predict the final fountain height as well as the width, velocity and buoyancy in the upflow and downflow. In that investigation, only the predictions of the fountain height were compared with experimental data, as measurements of the internal fountain structure did not become available until the study by Mizushina *et al.* (1982).

In this investigation, we present a new model of a turbulent fountain which builds on the ideas developed by McDougall (1981), but in which we consider an alternative

formulation for the entrainment between the upflow and the downflow. In § 2 we develop a theoretical model for an axisymmetric fountain in a homogeneous environment, and compare the numerical predictions with experimental measurements. In § 3, we extend this model to describe axisymmetric fountains in a stratified fluid, and compare the results with further experimental measurements. Our conclusions are summarized in § 4.

2. The model and equations in a homogeneous environment

In this section we focus on developing a simple yet effective model of a turbulent fountain in a homogeneous fluid. In § 2.1, we review the fountain model presented by McDougall (1981), and outline the differences in our analysis. We present a general form of the entrainment equations which includes two formulations of the buoyant body forces acting on the flow. Then, in § 2.2 we discuss two alternative formulations to quantify the entrainment between the upflow, downflow and environment. The numerical method used to solve the entrainment equations is introduced in § 2.3, and the results of the model are compared with experimental data in § 2.4.

2.1. *The model*

Immediately after injecting the heavy source fluid, the rising, jet-like flow mixes directly with the ambient fluid (figure 2*a*). The changing width, b, fluid velocity, u, and buoyant acceleration, Δ, in this initial flow can be quantified using the entrainment equations of Morton *et al.* (1956):

$$\frac{\mathrm{d}}{\mathrm{d}z}(b^2u) = 2\alpha bu, \quad \frac{\mathrm{d}}{\mathrm{d}z}(b^2u^2) = b^2\Delta, \quad \frac{\mathrm{d}}{\mathrm{d}z}(b^2u\Delta) = 0, \tag{2.1}$$

where $\Delta = (g/\rho_o)(\rho_f - \rho_o)$, g is the gravitational acceleration, ρ_o is the density of the ambient fluid, ρ_f is the density of the fluid in the fountain, z is the height above the source and α is the entrainment coefficient, which quantifies the mixing of ambient fluid into the turbulent flow. These equations rely on the entrainment assumption, which states that the mean inflow velocity is proportional to the local mean upflow velocity (Turner 1973, 1986). To simplify the entrainment equations, 'top hat' profiles of velocity and buoyancy are used to represent average quantities across the flow. From a solution of (2.1), the initial height of the fountain, z_i, is determined to be the point at which the velocity of the upflow becomes equal to zero. Although the predicted upflow radius goes to infinity at z_i, this definition of the top of the fountain has been shown to agree well with experimental measurements (Bloomfield & Kerr 1998).

The first complication we must consider in modelling a fountain is the reversal of the fluid after the initial height has been reached. McDougall (1981) introduced a method of dealing with the fluid reversal in which the numerical solution was terminated when the Froude number of the flow, defined as $Fr = u/(b\Delta)^{1/2}$, falls to $Fr = \sqrt{2}$. The rising fluid was then assumed to turn around under the action of the buoyancy, but without any additional mixing. This behaviour was modelled using a control volume comprising a cylinder of height h with a hemispherical cap of radius r (figure 3*a*). However, the ratio of h/r was an additional free parameter in his model. To avoid the necessity of including more free parameters in our analysis, we continue to define the top of the fountain as the point where the fluid velocity falls to zero (figure 3*b*). The reversal of fluid is modelled by assuming that as the fluid reaches a terminal height, it forms a ring at the outer edge of the upflow. From this circular

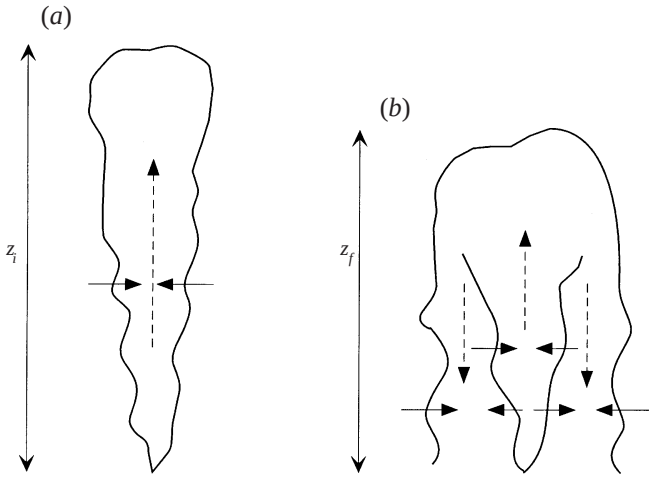

FIGURE 2. Schematic representation of a turbulent fountain (*a*) as the flow reaches an initial height and (*b*) after the fluid has reversed direction to form a downflow, and the initial height is reduced to a final, steady value. The dashed arrows indicate the flow direction, while the solid arrows indicate the directions of turbulent entrainment between the upflow, downflow and environment.

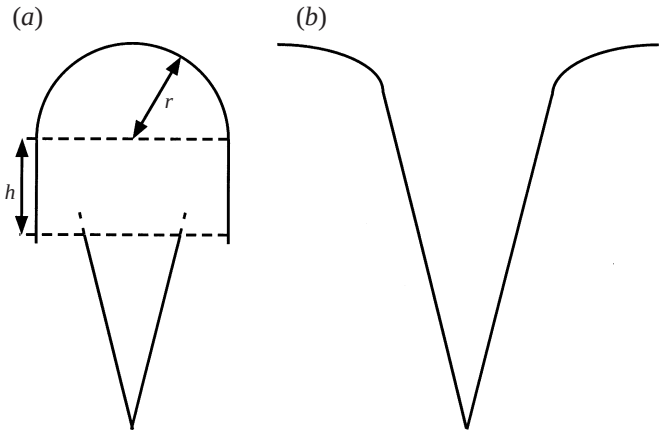

FIGURE 3. Comparison between the two methods of finding the fountain height as outlined (*a*) by McDougall (1981) and (*b*) in this study.

line source, the downflow forms as a line plume (Baines *et al.* 1990; Bloomfield & Kerr 1999) in which the fluxes of volume and buoyancy are distributed around a ring, giving the fountain its typical structure – a central upflow surrounded by an annular downflow (figure 2*b*).

Once the downflow has formed, our model must include the mixing that is indicated in figure 2(*b*) – fluid from the downflow is entrained into the upflow, while fluid is entrained into the downflow from both the upflow and the environment. We define separate properties for the upflow and the downflow, indicated by the subscripts u and d, respectively. The fluxes of volume, momentum and buoyancy are therefore

$$\left.\begin{aligned} Q_u &= \pi b_u^2 u_u, & Q_d &= \pi(b_d^2 - b_u^2)u_d, \\ M_u &= \pi b_u^2 u_u^2, & M_d &= \pi(b_d^2 - b_u^2)u_d^2, \\ F_u &= \pi b_u^2 u_u \Delta_u, & F_d &= \pi(b_d^2 - b_u^2)u_d \Delta_d. \end{aligned}\right\} \tag{2.2}$$

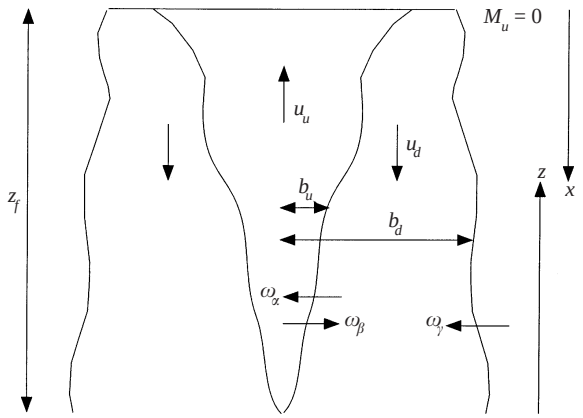

FIGURE 4. Model of a turbulent fountain, indicating the various quantities and properties that are included in the equations.

The terms for the buoyant acceleration are defined to be $\Delta_u = (g/\rho_o)(\rho_o - \rho_u)$ and $\Delta_d = (g/\rho_o)(\rho_d - \rho_o)$, with ρ_u and ρ_d the fluid densities in the upflow and downflow, respectively. The different signs of Δ_u and Δ_d here indicate whether the buoyant acceleration is opposing the motion ($\Delta_u < 0$), or whether it is in the direction of motion ($\Delta_d > 0$). To simplify the theoretical model, upflow quantities are measured at distances from the source, z, and downflow variables are measured at distances from the top of the fountain, x. The relevant fountain properties are illustrated in figure 4.

At this stage, we make no assumptions about the rate of entrainment into the upflow or downflow of the fountain, choosing instead to simply define ω_α as the velocity of entrainment into the upflow, ω_β as the entrainment velocity of fluid entering the downflow from the upflow, and ω_γ as the velocity of entrainment for ambient fluid mixed into the downflow (see figure 4). The choice of the relevant velocity scales on which to base ω_α, ω_β and ω_γ, and the consequences of this decision, are discussed in § 2.2.

In his theoretical model of a turbulent fountain, McDougall (1981) derived two sets of entrainment equations, based on two different assumptions about how the body forces affect the upflow and downflow. In both formulations, the equations for the conservation of volume and buoyancy fluxes were given by

$$\frac{\mathrm{d}}{\mathrm{d}z}(b_u^2 u_u) = 2b_u\omega_\alpha - 2b_u\omega_\beta, \tag{2.3a}$$

$$\frac{\mathrm{d}}{\mathrm{d}x}([b_d^2 - b_u^2]u_d) = 2b_d\omega_\gamma - 2b_u\omega_\alpha + 2b_u\omega_\beta, \tag{2.3b}$$

for the upflow and downflow volume fluxes, respectively, and

$$\frac{\mathrm{d}}{\mathrm{d}z}(b_u^2 u_u \Delta_u) = -2b_u\omega_\alpha\Delta_d - 2b_u\omega_\beta\Delta_u, \tag{2.4a}$$

$$\frac{\mathrm{d}}{\mathrm{d}x}([b_d^2 - b_u^2]u_d\Delta_d) = -2b_u\omega_\alpha\Delta_d - 2b_u\omega_\beta\Delta_u, \tag{2.4b}$$

for the upflow and downflow buoyancy fluxes.

In the first of his formulations for the buoyant body forces, McDougall (1981) assumed that the pressure gradient everywhere is hydrostatic and that the surfaces of constant pressure remain horizontal throughout the environment, the upflow and the downflow. In that case, the buoyant body forces accelerating the upflow depend only

on the density difference between the fluid in the upflow and that of the environment – that is, on Δ_u. This assumption leads to the following equations for the conservation of momentum flux in the upflow and the downflow:

$$\frac{\mathrm{d}}{\mathrm{d}z}(b_u^2 u_u^2) = b_u^2 \Delta_u - 2b_u \omega_\alpha u_d - 2b_u \omega_\beta u_u, \tag{2.5}$$

$$\frac{\mathrm{d}}{\mathrm{d}x}([b_d^2 - b_u^2] u_d^2) = [b_d^2 - b_u^2]\Delta_d - 2b_u \omega_\alpha u_d - 2b_u \omega_\beta u_u. \tag{2.6}$$

In the second of his body force formulations, McDougall (1981) assumed that the body force acting on the upflow is the local density difference between the upflow and downflow, $\Delta_u + \Delta_d$, so that the equation for the conservation of momentum flux in the upflow is

$$\frac{\mathrm{d}}{\mathrm{d}z}(b_u^2 u_u^2) = b_u^2 \left(\Delta_u + \Delta_d - u_d \frac{\mathrm{d}u_d}{\mathrm{d}x} \right) - 2b_u \omega_\alpha u_d - 2b_u \omega_\beta u_u, \tag{2.7}$$

where the term $u_d(\mathrm{d}u_d/\mathrm{d}x)$ is due to the acceleration of the frame of reference fixed to the downflow. The assumption was then made that the total momentum flux across the fountain should also be conserved, so that

$$\frac{\mathrm{d}}{\mathrm{d}z}(b_u^2 u_u^2) - \frac{\mathrm{d}}{\mathrm{d}x}([b_d^2 - b_u^2] u_d^2) = b_u^2 \Delta_u - [b_d^2 - b_u^2]\Delta_d. \tag{2.8}$$

Equations (2.8) and (2.7) then give

$$\frac{\mathrm{d}}{\mathrm{d}x}([b_d^2 - b_u^2] u_d^2) = [b_d^2 - b_u^2]\Delta_d + b_u^2 \left(\Delta_d - u_d \frac{\mathrm{d}u_d}{\mathrm{d}x} \right) - 2b_u \omega_\alpha u_d - 2b_u \omega_\beta u_u. \tag{2.9}$$

McDougall (1981) numerically integrated his entrainment equations to obtain predictions for the height of the fountain, as well as the radius, fluid velocity and density of the upflow and downflow, and compared the results with experimental measurements. Due to the number of arbitrary approximations in his model, McDougall (1981) stated that he could not conclude 'with any degree of confidence' which of the two body force formulations corresponded closest with experiment. However, he did note that when 'best guess' values were used for his free parameters, the second formulation gave a more accurate prediction of the final fountain height. In this study, we will continue to consider both formulations for the body forces, which we call BFI and BFII.

The set of entrainment equations (i.e. (2.3) and (2.4), together with either (2.5) and (2.6), or (2.7) and (2.9)) are simplified by writing them in terms of the non-dimensional variables given by

$$\left.\begin{aligned} \tilde{z} &= M_o^{-3/4} F_o^{1/2} z, \quad \tilde{b} = M_o^{-3/4} F_o^{1/2} b, \\ \tilde{u} &= M_o^{1/4} F_o^{-1/2} u, \quad \tilde{\omega} = M_o^{1/4} F_o^{-1/2} \omega, \\ \tilde{\Delta} &= M_o^{5/4} F_o^{-3/2} \Delta. \end{aligned}\right\} \tag{2.10}$$

After some rearranging, and introducing the dimensionless fluxes of volume, $\tilde{Q} = \tilde{b}^2\tilde{u}$, momentum, $\tilde{M} = \tilde{b}^2\tilde{u}^2$, and buoyancy, $\tilde{F} = \tilde{b}^2\tilde{u}\tilde{\Delta}$, the final equations are

$$\frac{\mathrm{d}\tilde{Q}_u}{\mathrm{d}\tilde{z}} = 2\frac{\tilde{Q}_u}{\tilde{M}_u^{1/2}}(\tilde{\omega}_\alpha - \tilde{\omega}_\beta), \tag{2.11a}$$

$$\frac{\mathrm{d}\tilde{Q}_d}{\mathrm{d}\tilde{x}} = 2\frac{\tilde{Q}_u}{\tilde{M}_u^{1/2}}\left(\left(1+\frac{1}{A}\right)^{1/2}\tilde{\omega}_\gamma + \tilde{\omega}_\beta - \tilde{\omega}_\alpha\right), \tag{2.11b}$$

$$\frac{\mathrm{d}\tilde{F}_u}{\mathrm{d}\tilde{z}} = -2\frac{\tilde{Q}_u}{\tilde{M}_u^{1/2}}\left(\frac{\tilde{F}_d}{\tilde{Q}_d}\tilde{\omega}_\alpha + \frac{\tilde{F}_u}{\tilde{Q}_u}\tilde{\omega}_\beta\right), \tag{2.11c}$$

$$\frac{\mathrm{d}\tilde{F}_d}{\mathrm{d}\tilde{x}} = -2\frac{\tilde{Q}_u}{\tilde{M}_u^{1/2}}\left(\frac{\tilde{F}_d}{\tilde{Q}_d}\tilde{\omega}_\alpha + \frac{\tilde{F}_u}{\tilde{Q}_u}\tilde{\omega}_\beta\right), \tag{2.11d}$$

with

$$\frac{\mathrm{d}\tilde{M}_u^2}{\mathrm{d}\tilde{z}} = 2\tilde{Q}_u\tilde{F}_u - 4\tilde{M}_u^{3/2}\left(B\tilde{\omega}_\alpha + \tilde{\omega}_\beta\right), \tag{2.11e}$$

$$\frac{\mathrm{d}\tilde{M}_d^2}{\mathrm{d}\tilde{x}} = 2\tilde{Q}_d\tilde{F}_d - 4\tilde{M}_u^{1/2}\tilde{M}_d\left(B\tilde{\omega}_\alpha + \tilde{\omega}_\beta\right), \tag{2.11f}$$

for the first body force formulation, and

$$\frac{\mathrm{d}\tilde{M}_u^2}{\mathrm{d}\tilde{z}} = 2\tilde{Q}_u\tilde{F}_u + 4\tilde{M}_u^{3/2}\left(B\left(1+\frac{1}{A}\right)^{1/2}\tilde{\omega}_\gamma + \frac{AB-1}{1+A}\tilde{\omega}_\beta - B\tilde{\omega}_\alpha\right), \tag{2.11g}$$

$$\frac{\mathrm{d}\tilde{M}_d^2}{\mathrm{d}\tilde{x}} = 2\tilde{Q}_d\tilde{F}_d + 4\tilde{M}_u^{1/2}\tilde{M}_d\left(B\left(1+\frac{1}{A}\right)^{-1/2}\tilde{\omega}_\gamma + \frac{AB-1}{1+A}\tilde{\omega}_\beta - B\tilde{\omega}_\alpha\right), \tag{2.11h}$$

for the second body force formulation. In these equations,

$$A = \frac{\tilde{Q}_u^2\tilde{M}_d}{\tilde{Q}_d^2\tilde{M}_u} = \frac{\tilde{b}_u^2}{\tilde{b}_d^2 - \tilde{b}_u^2} \quad \text{and} \quad B = \frac{\tilde{Q}_u\tilde{M}_d}{\tilde{Q}_d\tilde{M}_u} = \frac{\tilde{u}_d}{\tilde{u}_u}. \tag{2.12}$$

2.2. *Entrainment*

The entrainment assumption in its general form states that the inflow velocity of entrained fluid at any height scales with some characteristic velocity in the flow at that height (Morton *et al.* 1956). In flows with a 'double' structure, such as coaxial jets (Morton 1962), bubble plumes (McDougall 1978; Asaeda & Imberger 1993) or fountains (McDougall 1981), it is not immediately obvious on which velocity scales the entrainment velocities should be based. We present here two alternative formulations for the entrainment.

2.2.1. *Entrainment formulation I (EI)*

The first formulation we consider is that proposed by Morton (1962) for coaxial jets, and subsequently used by McDougall (1981) in his theoretical modelling of a turbulent fountain. Morton (1962) argued that the supply of energy to the turbulence in the inner flow arose due to the difference in mean velocities between the inner and outer flows. Consequently, it was this velocity difference on which the rate of entrainment should be based. Similarly, he proposed that the turbulence in the outer flow arose as a result of the shear between this flow and the stationary environment, leading to the prediction that the rate of entrainment into the outer flow should scale with the mean velocity of that flow. In a turbulent fountain, these arguments lead to the prediction that

$$\omega_\alpha = \alpha(u_u + u_d), \quad \omega_\beta = \beta u_d, \quad \omega_\gamma = \gamma u_d, \tag{2.13}$$

with α, β and γ the relevant entrainment coefficients.

In this formulation, the shear between the two flows is assumed to affect only the inner flow. However, it is not obvious to us why the turbulence generated by the shear should be transferred in one direction only (i.e. inwards). We therefore introduce a second entrainment formulation in which the shear between the flows affects the turbulence in both inner and outer flows.

2.2.2. *Entrainment formulation II* (*EII*)

In this formulation, we argue that the total shear, $u_u + u_d$, should be partitioned (cf. Morton 1962) so that only the component containing upward velocities, $u_u/(u_u + u_d)$, affects the turbulence in the upflow, and the remaining component, $u_d/(u_u + u_d)$, feeds the turbulence in the downflow. The entrainment velocities therefore depend on the relevant fraction of the total shear, and are given by

$$\omega_\alpha = \alpha u_u, \quad \omega_\beta = \beta u_d, \quad \omega_\gamma = \gamma u_d. \tag{2.14}$$

Essentially, we have again assumed that the entrainment velocity scales with a velocity difference, although this time the shear is taken to be the difference between the mean fluid velocity in the flow and the mean velocity on the 'edge' of the flow under consideration. This approach is consistent with the commonly stated entrainment assumption in simple flows where the velocity on the edge of the flow is equal to that in the environment. In a fountain, however, the obvious position of the boundary between the upflow and downflow is the point at which the mean velocity is equal to zero (Mizushina *et al.* 1982, figure 7).

2.3. *The numerical method*

The starting conditions for the integration of the upflow equations are defined at a height z_o above the point source. This is necessary to avoid the infinite fluid velocity, $u_o = M_o/Q_o$, that would arise from a theoretical point source ($Q_o = 0$). To determine the values of $\tilde{Q}, \tilde{M}$ and $\tilde{F}$ at a height of $\tilde{z}_o = 0.01$, we note that near the source, the upflow is unaffected by either its negative buoyancy or the presence of the downflow (Bloomfield & Kerr 1999). From a solution of (2.1) for a jet ($\tilde{Q}_o = 0, \tilde{M}_o = 1, \tilde{F}_o = 0$), we find that $\tilde{Q}(\tilde{z}_o) = 2\alpha\tilde{z}_o$ and $\tilde{M}(\tilde{z}_o) = 1$. In a fountain, we then assume that $\tilde{F}$ is unchanged from its value at the source, so that $\tilde{F}(\tilde{z}_o) = -1$.

Initially there is no downflow ($\tilde{Q}_d = \tilde{M}_d = \tilde{F}_d = 0$) so that (2.11*a*) and (2.11*c*) together with either (2.11*e*) or (2.11*g*) reduce to the standard entrainment equations (2.1). These equations for the upflow are solved numerically using a routine based on a fourth-order Runge–Kutta scheme. The point at which the upflow momentum flux becomes equal to zero gives a value of the initial fountain height, $\tilde{z}_i$ (Morton 1959; Bloomfield & Kerr 1998). The values of the upflow volume flux, $\tilde{Q}_T$, and buoyancy flux, $\tilde{F}_T$, at this initial height are the starting conditions for $\tilde{Q}_d$ and $\tilde{F}_d$ at $\tilde{x} = 0$ ($\tilde{x}$ is measured from the top of the fountain). The conservation equations for the downflow (2.11*b*, 2.11*d* and either 2.11*f* or 2.11*h*) are then integrated from the top of the fountain to the starting point at $\tilde{z}_o$, using the previously determined values of $\tilde{Q}_u$, $\tilde{M}_u$ and $\tilde{F}_u$ at each height. These newly determined values for the fluxes in the downflow are then used in the next integration of the upflow equations. The point at which $\tilde{M}_u = 0$ in this iteration gives the first estimate of the reduced final height, $\tilde{z}_f$. This procedure is continued until the estimate of $\tilde{z}_f$ from subsequent iterations converges to a fixed value, which we take as our evaluation of the final fountain height.

$\tilde{z}_i$	$\tilde{z}_f$	$Fr_{\max}$	Reference
2.65 ± 0.36	1.85 ± 0.25	250	Turner (1966); Baines *et al.* (1990)
	1.76 ± 0.15	100	Mizushina *et al.* (1982)
2.32 ± 0.08	1.70 ± 0.17	65	Appendix

TABLE 1. Dimensionless values of the initial and final fountain heights from several experimental investigations.

2.4. *Results and comparison with experiments*

The method outlined above was used to determine the initial fountain height, $\tilde{z}_i$, as well as four values of the dimensionless fountain height, $\tilde{z}_f$, for the combinations of two body force formulations (BFI and BFII) and two entrainment formulations (EI and EII). The values obtained for $\tilde{z}_i$ and $\tilde{z}_f$ correspond to the experimentally determined constants in the expressions relating the fountain heights to the intrinsic length scale of $M_o^{3/4}F_o^{-1/2}$ (Turner 1966).

A number of investigators have measured $\tilde{z}_i$ and $\tilde{z}_f$ under a variety of conditions and for a range of Froude numbers, Fr, where $Fr = u_o/(r_o\Delta_o)^{1/2}$ (table 1). The most extensive measurements of the fountain height ($Fr < 250$) were presented by Baines *et al.* (1990), who obtained a value of $\tilde{z}_f = 1.85 \pm 0.25$ (where we have estimated the error from their experimental data). This data set included some experiments at relatively low Froude numbers ($Fr < 20$) made previously by Turner (1966), in which the ratio of the initial to final fountain height was found to be $\tilde{z}_i/\tilde{z}_f = 1.43$. Combining these two results gives an estimate of $\tilde{z}_i = 2.65 \pm 0.36$ for the initial fountain height. Some measurements of the final fountain height for Froude numbers up to $Fr = 100$ were made by Mizushina *et al.* (1982), who obtained a value of $\tilde{z}_f = 1.76 \pm 0.15$ (where we have once again estimated the error from their data set). We also note that some other investigations (e.g. McDougall 1981; Lindberg 1994) give values of $\tilde{z}_f$, but these studies do not carefully document the source conditions (i.e the position of the virtual source and the effective source radius). The variation in the reported values of $\tilde{z}_f$, and the limited measurements of $\tilde{z}_i$ motivated us to perform our own experiments (described in detail in the Appendix), from which we found that $\tilde{z}_i = 2.32 \pm 0.08$ and $\tilde{z}_f = 1.70 \pm 0.17$. Both our measurements and those of Mizushina *et al.* (1982) are somewhat lower than the results of Baines *et al.* (1990), although they do lie within the range of experimental scatter.

In the first iteration of the upflow equations, α is the only free parameter. It was found by Bloomfield & Kerr (1998) that a value of $\alpha = 0.085 \pm 0.01$ (which lies between the jet value of $\alpha = 0.076 \pm 0.004$ and the plume value of $\alpha = 0.117 \pm 0.006$ (Fischer *et al.* 1979; Rodi 1982) gave a good prediction of the initial height of a fountain in a stratified fluid. In a homogeneous fluid, the value of $\alpha = 0.085 \pm 0.01$ results in a numerical estimate of $\tilde{z}_i = 2.49 \pm 0.15$, which lies between the two experimentally determined values (see table 1) of $\tilde{z}_i = 2.65 \pm 0.38$ (Turner 1966) and $\tilde{z}_i = 2.32 \pm 0.08$ (Appendix).

By modelling the downflow as a line plume which encircles the upflow, we fix the entrainment coefficients β and γ at the value found for a line plume with top-hat profiles of velocity and buoyancy: $\beta = \gamma = 0.147$ (List 1982). The uncertainty in the entrainment coefficient for a line plume can be calculated from the results of Kotsovinos & List (1977) to be $\beta = \gamma = 0.147 \pm 0.014$. These values of β and γ

	Entrainment I (EI)	Entrainment II (EII)
Body force I (BFI)	$\tilde{z}_f = 1.07 \pm 0.09$	$\tilde{z}_f = 1.25 \pm 0.09$
Body force II (BFII)	$\tilde{z}_f = 1.20 \pm 0.10$	$\tilde{z}_f = 1.49 \pm 0.11$

TABLE 2. Numerical results for the fountain for the two body force formulations, and two entrainment formulations.

contrast those used by McDougall (1981), who incorrectly used Gaussian entrainment coefficients in entrainment equations which were developed assuming top-hat profiles.

The predictions of the final fountain height obtained from the combination of two entrainment formulations and two buoyant body force formulations (referred to hereinafter as BFIEI, BFIEII, BFIIEI and BFIIEII) are summarized in table 2, showing the variation in $\tilde{z}_f$ due to the uncertainty in the entrainment coefficients α, β and γ. All the numerical results underestimate the various experimental measurements, with the combination BFIIEII ($\tilde{z}_f = 1.49 \pm 0.11$) giving the result closest to the experimentally determined value.

To determine the sensitivity of the results to variations in β and γ, we first decreased β from the value for a plume to that for a jet ($\beta = 0.076$), while keeping γ fixed. This resulted in only a 0.5% decrease in the predicted fountain height. Decreasing β has two effects: first, less of the dense rising fluid is mixed into the downflow, so that the downflow remains lighter and therefore experiences a smaller downward acting buoyancy force; second, however, the decrease in the interaction with the upflow allows greater acceleration of the falling fluid. As varying β has a negligible effect on the predicted fountain height, it appears that these two effects essentially cancel each other out.

In contrast, when γ was also reduced to the jet value of $\gamma = 0.076$, the numerical estimate for the fountain height dropped by approximately 20%. In this case, mixing with the stationary environment does not affect the momentum of the downflow, so the only effect of decreasing the entrainment from the environment is to give a denser and therefore more accelerated downflow.

In addition to the comparisons for the final fountain height, the numerical predictions of the upflow and downflow properties can also be compared with the experimental measurements of Mizushina *et al.* (1982). In figure 5(*a*), the numerical results from all four formulations are compared with the experimental measurements of the upflow and downflow radius (Mizushina *et al.* 1982). Despite the numerical results for the upflow and downflow radius becoming unrealistic near the top of the fountain, the results from all four formulations lie within the range of experimental scatter. The predictions for the outer radius are much better than those obtained by McDougall (1981), who stated that his numerical results for the fountain radius were approximately half of the experimentally measured radius.

Figure 5(*b*) shows that for all four formulations, our numerical results for the upflow velocity are in excellent agreement with the centreline velocities measured by Mizushina *et al.* (1982). Near the top of the fountain, the numerical and experimental

FIGURE 5. Comparison of the numerical results with experimental data (symbols) of Mizushina *et al.* (1982) for (*a*) the upflow and downflow radius, (*b*) the upflow velocity and (*c*) the upflow buoyancy also including some experimental results of Seban *et al.* (1978). Shown are the numerical results for the four different formulations: BFIEI (· · · ·), BFIIEI (– · – · –), BFIEII (- - - -) and BFIIEII (——).

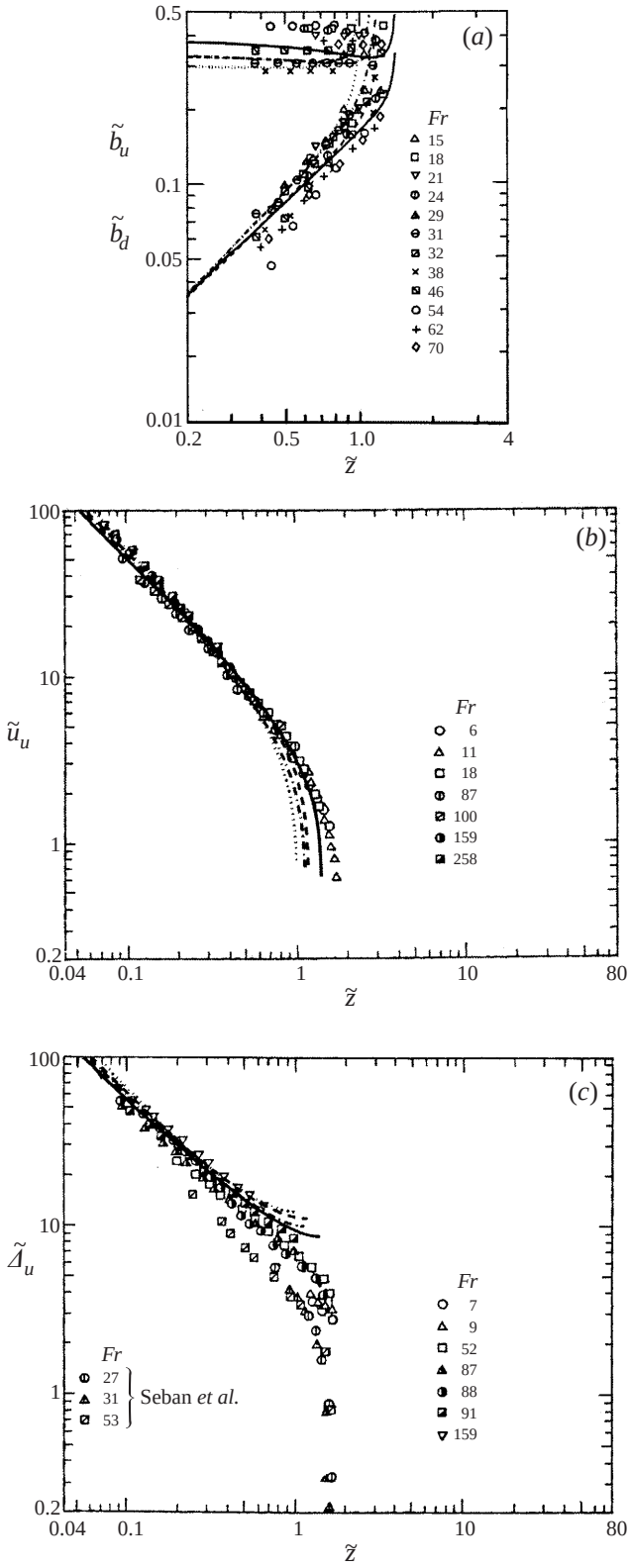

FIGURE 5. For caption see facing page.

results diverge, as the different calculations of the fountain height become apparent. The numerical predictions of the upflow buoyancy shown in figure 5(*c*) slightly overestimate the centreline measurements, with a significant deviation near the top of the fountain. The rapid decrease in buoyancy to the ambient value near the top of the fountain in the experimental data is due to the fluctuations in the fountain height, where measurements of the upflow buoyancy are a time average of the buoyancy of the fountain fluid and that of the ambient fluid.

The calculated velocities and buoyancies in the fountain downflow are plotted in figures 6(*a*) and 6(*b*), respectively. Figure 6(*a*) shows that all the formulations predict a rapid increase in the downflow velocity from zero at the top of the fountain to a maximum near $\tilde{z} = 0.6\tilde{z}_f$, followed by a decrease of 10–15% down to $\tilde{z} = 0$. The only experimental measurements of the downflow velocity with which to compare these theoretical results were made by Mizushina *et al.* (1982, figure 7), who measured the ratio u_d/u_u at two different heights. These measurements, when combined with their data for the upflow velocity (see figure 5*b*), indicate that the downflow velocity decreased by about $30 \pm 15\%$ from $\tilde{z} = 0.54\tilde{z}_f$ to $\tilde{z} = 0.24\tilde{z}_f$, where we have estimated the error from the scatter in the experimental data. We note that this measured decrease is somewhat greater than our calculations of a 5–10% decrease in velocity between these heights.

Figure 6(*b*) shows that the calculated buoyancy decreases by 50–60% between the top of the fountain and the source, and the magnitude of the buoyancy depends on the formulation used. These calculations can also be compared with the experimental data of Mizushina *et al.* (1982). From their measurements of the ratio Δ_d/Δ_u (Mizushina *et al.* 1982, figure 8), together with their data for the upflow buoyancy (see figure 5*c*), we estimate that the downflow buoyancy decreased by about $25 \pm 20\%$ from $\tilde{z} = 0.54\tilde{z}_f$ to $\tilde{z} = 0.24\tilde{z}_f$. We note that this decrease is comparable to our calculated buoyancy decrease of approximately 20% between these heights.

In summary, the calculated fountain properties agree well with the available experimental measurements over most of the fountain height. The largest deviations arise near the top of the fountain, which probably reflects the fact that elements of fluid come to rest at different heights, in contrast to our simple assumption that all the fluid comes to rest at the same height (cf. figure 4).

3. Application of the model to a stratified environment

In this section, we extend our theoretical model to describe a turbulent fountain in a linearly stratified environment. We outline the changes to the model in § 3.1, before comparing the model results with experimental measurements in § 3.2. In § 3.2.1, the equations are solved in the limiting case of a zero buoyancy flux at the source, before we proceed in § 3.2.2 to solve the equations for any source conditions.

3.1. *The revised model and equations*

In a previous experimental study of fountains in a linearly stratified fluid, Bloomfield & Kerr (1998) measured the fountain properties in terms of a dimensionless parameter $\sigma = M_o^2 N^2 / F_o^2$, where $N^2 = (-g/\rho_o)\mathrm{d}\rho/\mathrm{d}z$ is a measure of the strength of the stratification, g is the gravitational acceleration, ρ_o is the ambient density at the base of the tank and $\rho(z)$ is the ambient density at a height z above the base of the tank. In terms of this parameter σ, the fountain behaviour varies from that observed in a homogeneous fluid ($\sigma = 0$) to the case where the density of the source fluid is equal to the ambient at the base of the stratification ($F_o = 0$, $\sigma = \infty$). In contrast to

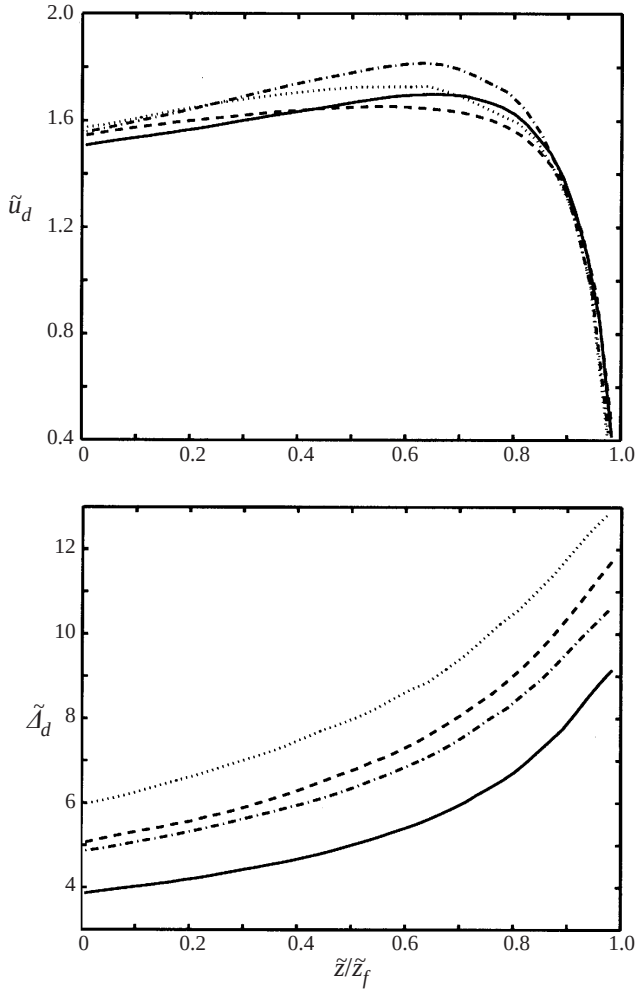

FIGURE 6. Numerical calculations of the (*a*) velocity and (*b*) buoyancy in the downflow for each of the four formulations (line styles as for figure 5).

the $\sigma = 0$ behaviour described in § 2.1, when $\sigma = \infty$, the density of the downflow becomes equal to the ambient density at some height above the source. At this height of neutral buoyancy, the downflow still has some momentum, so that the flow overshoots slightly before intruding as a thin spreading layer (figure 7). In a stratified fluid, therefore, there are two distinct regimes of behaviour which are represented by basal and intermediate spreading. The transition between these regimes occurs at a critical value of $\sigma_c = 5.0$, so that for $\sigma < \sigma_c$, basal spreading occurs, while for $\sigma > \sigma_c$, intermediate intrusion takes place (Bloomfield & Kerr 1998).

Despite the differences in the qualitative behaviour when intermediate spreading occurs, the basic fountain model remains unchanged from that presented in § 2.1: a central jet-like upflow is surrounded by an annular plume-like downflow. Consequently, the equations for the conservation of volume flux (2.3*a*, *b*) and momentum flux ((2.5) and (2.6) or (2.7) and (2.9)) are similarly unchanged. In an ambient density gradient, however, the conservation of buoyancy flux in the upflow and downflow,

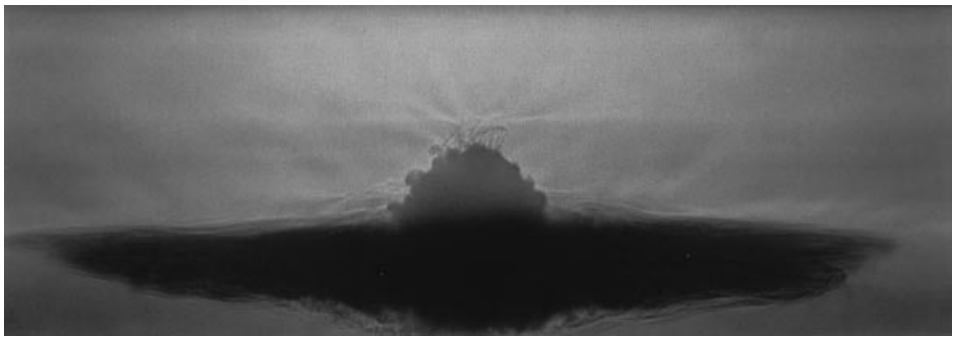

FIGURE 7. Photograph of an axisymmetric fountain in a linearly stratified environment, when the flow has a zero buoyancy flux at the source ($\sigma = \infty$).

respectively, becomes

$$\frac{\mathrm{d}}{\mathrm{d}z}(b_u^2 u_u \Delta_u) = -N^2 b_u^2 u_u - 2b_u \omega_\alpha \Delta_d - 2b_u \omega_\beta \Delta_u, \tag{3.1a}$$

$$\frac{\mathrm{d}}{\mathrm{d}x}([b_d^2 - b_u^2] u_d \Delta_d) = -N^2 [b_d^2 - b_u^2] u_d - 2b_u \omega_\alpha \Delta_d - 2b_u \omega_\beta \Delta_u, \tag{3.1b}$$

where the buoyancies Δ_u and Δ_d are now defined by $\Delta_u = (g/\rho_o)(\rho(z) - \rho_u)$ and $\Delta_d = (g/\rho_o)(\rho_d - \rho(z))$, with $\rho(z)$ the ambient density at a height z above the source, and $\rho_o = \rho(0)$.

The model now includes the possibility of intermediate spreading. Previously, Bloomfield & Kerr (1998) obtained a numerical estimate of the spreading height by calculating the fluid density at the initial fountain height, and finding where fluid of this density would intrude into the environment. We extend that method here to obtain a better approximation, although there are three outcomes of the model. In a strong gradient ($\sigma \to \infty$), the solution for the downflow buoyancy flux falls to zero at an intermediate height, and the momentum flux is reduced to zero closer to the source. An approximation for the spreading height is obtained by calculating the fluid density at the point where the downflow momentum flux becomes equal to zero, and finding where the fluid of this density would intrude in the environment (figure 8*a*). As the conditions approach the transition between the two regimes of behaviour ($\sigma \approx \sigma_c$), the buoyancy flux falls to zero above the source but the downflow still has momentum at the base (figure 8*b*). In this case, the density of the downflow as it reaches the base is calculated, and this density used to determine the spreading height. In the third case ($\sigma \to 0$), neither the buoyancy or momentum fluxes in the downflow reach zero, and basal spreading occurs (figure 8*c*).

In the experimental study of fountains in a stratified fluid (Bloomfield & Kerr 1998), the source characteristics were analysed in detail, and it was found that the flow was turbulent from the source and the virtual point source was located 1 cm below the base of the tank. The numerical integration of the entrainment equations is therefore started at the level of the actual source ($z_o = 0.01$ m) with an effective radius of $r_o = 4.16 \times 10^{-3}$ m and a non-zero volume flux. As we are no longer assuming flow from a point source, the entrainment equations must be solved in their dimensional form ((2.3) and (3.1) together with either (2.5) and (2.6), or (2.7) and (2.9)).

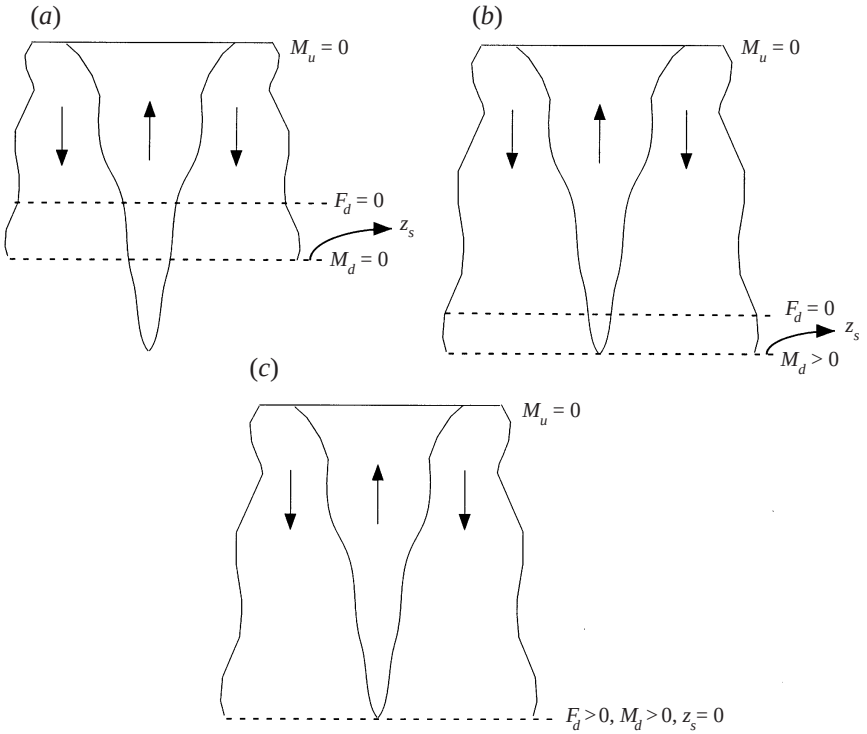

FIGURE 8. To determine the spreading height in a stratified fluid either (*a*) the density of the downflow is found at the point where the momentum flux falls to zero, and the level where this fluid would intrude is calculated, or (*b*) the density of the now buoyant falling fluid when it reaches the base is determined, and the level where this fluid would intrude is calculated, or (*c*) the downflow reaches the base still heavier than its environment and basal spreading occurs.

3.2. *Results*

In § 2.4, we discussed the numerical results for the special case of a homogeneous environment ($\sigma = 0$). Before proceeding to apply the model to flows with any value of σ, we first consider the other limiting case of $\sigma \to \infty$, which has been studied in detail experimentally.

3.2.1. *Theoretical results for* $\sigma = \infty$

It has been shown that when $\sigma \to \infty$, the fountain heights are given by $z = CM_o^{1/4}N^{-1/2}$ with experimentally determined constants C_i, C_f and C_s for the initial, final and spreading heights, respectively (Bloomfield & Kerr 1998). To obtain a numerical prediction of these constants, the slope of a plot of the calculated fountain heights against $M_o^{1/4}N^{-1/2}$ was obtained. The value of N was fixed at $N = 1\,\mathrm{s}^{-1}$, while M_o was varied between 5×10^{-8} and $1 \times 10^{-4}\,\mathrm{m}^4\,\mathrm{s}^{-2}$. The region corresponding to fountains less than 2 cm in height was excluded, as the effect of a finite source is considerable at small heights. Using an entrainment coefficient of $\alpha = 0.085 \pm 0.010$ (Bloomfield & Kerr 1998), the numerical prediction of $C_i = 3.29 \pm 0.16$ agrees well with the experimentally determined value of $C_i = 3.25 \pm 0.17$.

The final and spreading heights were calculated for the two body force formulations and the two entrainment formulations, using $\alpha = 0.085 \pm 0.010$ and $\beta = \gamma = 0.147 \pm 0.014$, with the results shown in table 3. For the homogeneous results, BFIIEII (using

	Entrainment I	Entrainment II
Body force I	$C_f = 2.80 \pm 0.15$ $C_s = 1.43 \pm 0.08$	$C_f = 2.98 \pm 0.12$ $C_s = 1.50 \pm 0.06$
Body force II	$C_f = 2.94 \pm 0.15$ $C_s = 1.57 \pm 0.08$	$C_f = 3.23 \pm 0.16$ $C_s = 1.60 \pm 0.10$

TABLE 3. Numerical predictions for the constants in the expression $z = C \times M_o^{1/4} N^{-1/2}$ for the final (C_f) and spreading (C_s) heights.

$\alpha = 0.076$) underestimated the final height. Here, this combination predicts a final height of $C_f = 3.23 \pm 0.16$ and a spreading height of $C_s = 1.60 \pm 0.10$, both of which slightly overestimate the experimentally determined values of $C_f = 3.00 \pm 0.23$ and $C_s = 1.53 \pm 0.10$, respectively (Bloomfield & Kerr 1998). The closest agreement with the experimental results is obtained using BFIEII ($C_f = 2.98 \pm 0.12$, $C_s = 1.53 \pm 0.06$). However, as all of the formulations predict final and spreading heights which lie within the error bars of the experimentally determined results, these results do not clearly support any particular one of the formulations. This result is not unexpected, as Bloomfield & Kerr (1998) showed that the distance over which the upflow and downflow interact clearly affects the amount by which the final fountain height is reduced from the initial value (Bloomfield & Kerr 1998, figure 6*c*). In a homogeneous fluid, $\tilde{z}_i/\tilde{z}_f = 1.43$ (Turner 1966), but this ratio falls to $\tilde{z}_i/\tilde{z}_f = 1.05$ as the spreading height reaches a maximum. With such a small difference between $\tilde{z}_i$ and $\tilde{z}_f$, the scope for any differences between the four formulations is similarly reduced.

3.2.2. *Theoretical results for* $0 < \sigma < \infty$

Of the four possible model variations, those including the second entrainment formulation gave the best results at $\sigma = 0$, while little difference was observed between the formulations at $\sigma = \infty$. We therefore now use the second entrainment formulation (variations BFIEII and BFIIEII) to model the fountain for the full range of σ.

Bloomfield & Kerr (1998) used a dimensional argument to show that a general expression for the fountain heights in a stratified fluid is $z = f(\sigma) M_o^{3/4} F_o^{-1/2}$, where $f(\sigma)$ is different for the initial, final and spreading heights. Experimental measurements of the fountain heights, non-dimensionalized by the homogeneous length scale, $M_o^{3/4} F_o^{-1/2}$, were plotted against σ to show $f(\sigma)$ for the three heights. Numerical predictions for $f(\sigma)$ for the initial, final and spreading heights were obtained for $\sigma = 10^{-1}$–10^4 by fixing $F_o = 5 \times 10^{-5}\,\mathrm{m^4\,s^{-3}}$ and varying M_o from 7×10^{-5} to $3 \times 10^{-3}\,\mathrm{m^4\,s^{-2}}$ and N between 0.2 and $1.6\,\mathrm{s^{-1}}$. Tests of the program showed that for any value of σ, $f(\sigma)$ was independent of the actual values of M_o, F_o and N. The numerical results using BFIEII and BFIIEII with $\alpha = 0.085$ and $\beta = \gamma = 0.147$ are shown in comparison with the experimental results in figure 9. Although the results using BFIIEII (figure 8*b*) overestimate the fountain heights as $\sigma \to \infty$, this formulation gives the better prediction of the experimental results over the full range of σ. These graphs also show the range of σ corresponding to the three variations in the modelling of the downflow that were illustrated in figure 8.

From the numerical results, it is also possible to predict the critical value of σ_c which quantifies the transition between basal and intermediate spreading. Using

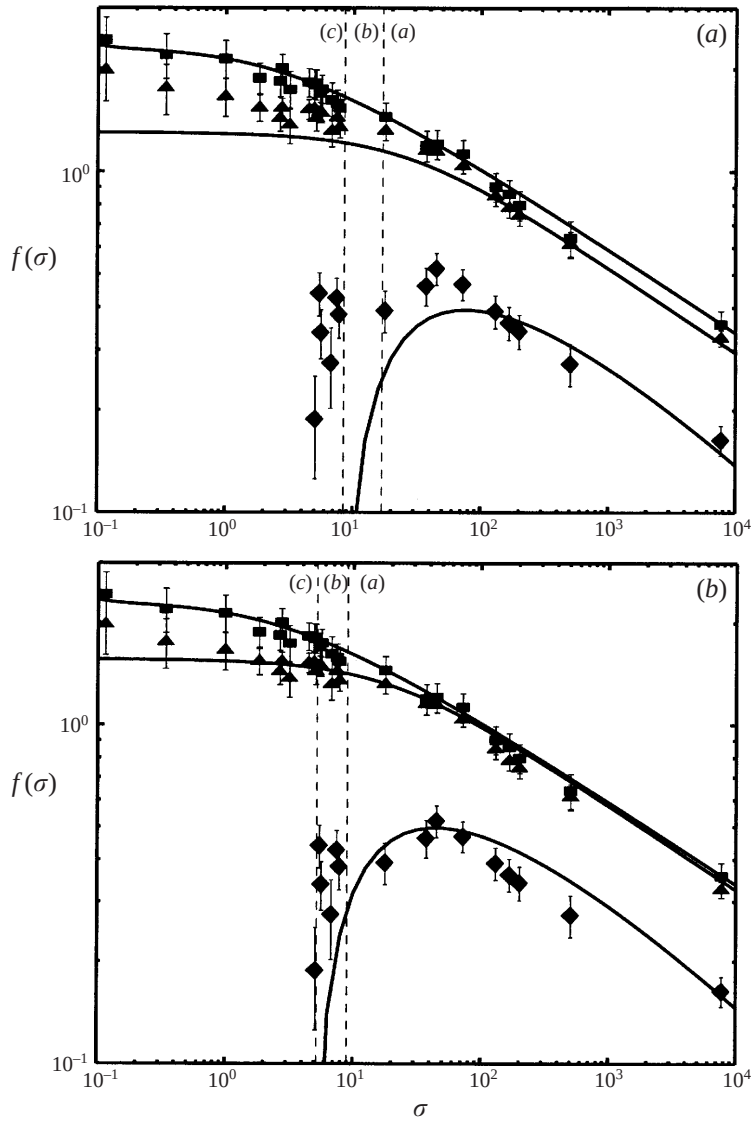

FIGURE 9. Comparison between the experimental measurements of $f(\sigma)$ for the initial, final and spreading heights with the numerical predictions obtained using $\alpha = 0.085$, $\beta = \gamma = 0.147$ in the formulations: (*a*) BFIEII and (*b*) BFIIEII. Also shown on the figures are the three regimes of behaviour corresponding to the different methods of determining the spreading height.

BFIEII gives $\sigma_c = 8.5$, while the prediction of $\sigma_c = 5.2$ obtained using BFIIEII is in much better agreement with the experimentally determined value of $\sigma_c = 5.0 \pm 0.1$.

4. Conclusions

We have developed a theoretical model of an axisymmetric turbulent fountain, in which a set of entrainment equations is used to quantify the turbulent mixing between the upflow, the downflow and the environment. The derivation of the entrainment equations relied on the replacement of unknown profiles of velocity and buoyancy

with average 'top-hat' profiles. In our modelling, we have focused on the effects that different formulations of the body forces and entrainment velocities have on the fountain properties. In the two body force formulations considered, the buoyant acceleration of the upflow was measured relative to either the stationary environment (BFI) or to the accelerating downflow (BFII). In the two entrainment formulations, the entrainment into the upflow was quantified using either the velocity difference between the upflow and downflow (EI) or the velocity of the upflow (EII).

All four variations of the entrainment equations were integrated numerically to calculate the initial, final and spreading heights of the fountain, as well as the radius, velocity and buoyancy of the upflow and downflow. In a homogeneous fluid, the calculated final fountain heights were all lower than the experimental measurements, with the differences between theory and experiment ranging from about 40% (using BFI and EI) to about 15% (using BFII and EII). This difference between the model and experimental measurements probably reflects the fact that both the assumed top-hat profiles and the model pictured in figure 4 are only rough descriptions of the actual behaviour near the top of the fountain.

The theoretical model also gave predictions of the velocity and buoyancy in the upflow, as well as the radius of the upflow and downflow. These calculated properties were compared with all available experimental data, and were found to be in good agreement.

In a stratified fluid, the equations were integrated to give the initial, final and spreading heights as a function of the dimensionless parameter, σ, as it varies from $\sigma = 0$ (homogeneous fluid) to $\sigma \to \infty$ (stratified fluid with zero buoyancy flux at the source). As the spreading height rises to an intermediate level (at larger values of σ), the interaction between the upflow and downflow decreases, and consequently there is little difference between the four formulations at large values of σ. The best agreement over the full range of σ was therefore obtained using the combination of body force and entrainment formulations that best predicted the fountain heights in a homogeneous fluid (BFII and EII).

Our original aim was to develop a theoretical model which could be used to calculate the fountain properties in an arbitrary density gradient. The model we have presented is accurate to about 15% in a homogeneous fluid, with the accuracy increasing to about 5% in a linearly stratified fluid. In an arbitrary density gradient, we therefore expect the model presented to give reasonably accurate predictions of the fountain properties, especially in cases where intermediate intrusion occurs. One important situation where the theory is needed is in a confined stratified environment (Bloomfield & Kerr 1999), where the ambient density gradient continuously evolves with time.

We thank Tony Beasley, Derek Corrigan and Ross Wylde-Browne for their technical assistance with the experiments. We also thank Stewart Turner for his helpful comments and for providing us with the photograph shown in figure 1. One of the experiments was performed with the aid of Melanie Cooper. The financial support of an Australian Research Council Fellowship (for R. K.) and that of a Jaeger Scholarship and Australian Postgraduate Award (for L. B.) are gratefully acknowledged.

Appendix. Experiments

To measure the fountain heights, we used the same experimental apparatus and setup that was previously employed by Bloomfield & Kerr (1998) to investigate

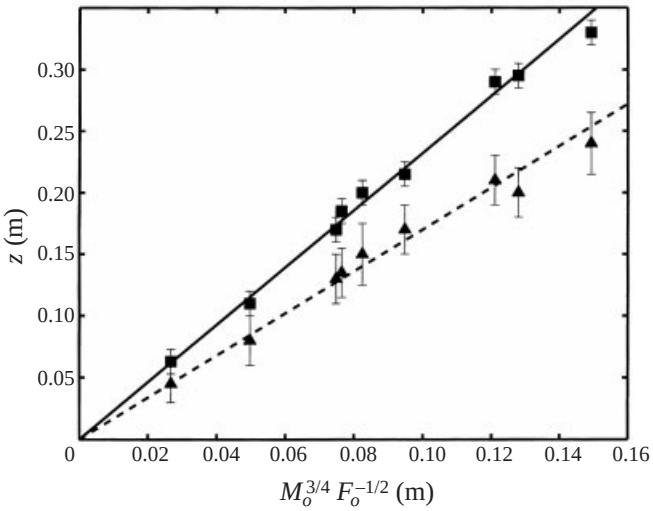

FIGURE 10. Experimental measurements of the initial (■) and final (▲) fountain heights in a homogeneous fluid. The heights are plotted against the length scale, $M_o^{3/4} F_o^{-1/2}$ giving values of $\tilde{z}_i = 2.32 \pm 0.08$ and $\tilde{z}_f = 1.70 \pm 0.11$.

turbulent fountains in a stratified fluid. A tank 70 cm deep and 40 cm × 40 cm in cross-section was filled with tap water. Source fluid of varying density, ρ_i, was placed in a 20 l bucket which was raised 1.5 m higher than the main tank. The flow rate resulting from this gravitational head was adjusted with a valve and measured with a flow meter to an accuracy of 1–4%. The source fluid was injected upwards from the base of the tank through a tube with an 8.8 mm inner diameter. Two sets of crosshairs were aligned and positioned 3 mm and 44 mm from the nozzle outlet to ensure that the flow was turbulent from the source. To quantify the effect of these crosshairs, Bloomfield & Kerr (1998) used measurements of the position of the descending front formed by a jet impinging on the free surface to determine an effective source radius, r_e. For fully laminar flow, $r_e = \sqrt{3}\, r_o/2$, while for turbulent flow, $r_e = r_o$. Careful measurements by Bloomfield & Kerr (1998) indicated that the effective source radius was $r_e = 4.16 \pm 0.23$ mm, and hence that the flow was almost fully turbulent from the source. In addition, the virtual source was found to lie 1.0 ± 0.2 cm below the base of the tank. One further experiment was performed with a 3.2 mm diameter nozzle for which it was found that $r_e = 1.46 \pm 0.08$ mm with the virtual source coinciding with the nozzle outlet.

In total, we performed nine experiments for Froude numbers in the range 10–70. The measured initial and final heights of the fountain above the virtual source are plotted in figure 10 against the length scale, $M_o^{3/4} F_o^{-1/2}$. The average value of $\tilde{z}_i$ and $\tilde{z}_f$ was calculated to give values, within two standard deviations, of $\tilde{z}_i = 2.32 \pm 0.08$ and $\tilde{z}_f = 1.70 \pm 0.17$.

REFERENCES

ASAEDA, T. & IMBERGER, J. 1993 Structure of bubble plumes in linearly stratified environments. *J. Fluid Mech.* **249**, 35–57.

BAINES, W. D., TURNER, J. S. & CAMPBELL, I. H. 1990 Turbulent fountains in an open chamber. *J. Fluid Mech.* **212**, 557–592.

Bloomfield, L. J. & Kerr, R. C. 1998 Turbulent fountains in a stratified fluid. *J. Fluid Mech.* **358**, 335–356.

Bloomfield, L. J. & Kerr, R. C. 1999 Turbulent fountains in a confined stratified fluid. *J. Fluid Mech.* **389**, 27–54.

Campbell, I. H. & Turner, J. S. 1989 Fountains in magma chambers. *J. Petrol.* **30**, 885–923.

Fischer, H. B., List, E. J., Koh, R. C. Y., Imberger, J. & Brooks, N. H. 1979 *Mixing in Inland and Coastal Waters.* Academic.

Koh, R. C. Y. & Brooks, N. H. 1975 Fluid mechanics of waste-water disposal in the ocean. *Ann. Rev. Fluid Mech.* **7**, 187–211.

Kotsovinos, N. E. & List, E. J. 1977 Plane turbulent buoyant jets. Part I: Integral properties. *J. Fluid Mech.* **81**, 25–44.

Lindberg, W. R. 1994 Experiments on negatively buoyant jets, with and without cross-flow. In *Recent Research Advances in the Fluid Mechanics of Turbulent Jets and Plumes*, pp. 131–145. Kluwer.

Lindgerg, W. R. & Petersen, J. D. 1991 Negatively buoyant jet (or plume) with application to snowplow exit flow behavior. *Transportation Research Record* **1304**, 219–229.

List, E. J. 1982 Turbulent jets and plumes. *Ann. Rev. Fluid. Mech.* **14**, 189–212.

McDougall, T. J. 1978 Bubble plumes in stratified environments. *J. Fluid Mech.* **85**, 655–672.

McDougall, T. J. 1981 Negatively buoyant vertical jets. *Tellus* **33**, 313–320.

Mizushina, T., Ogino, F., Takeuchi, H. & Ikawa, H. 1982 An experimental study of vertical turbulent jet with negative buoyancy. *Wärme-und Stoffübertragung* **16**, 15–21.

Morton, B. R. 1959 Forced plumes. *J. Fluid Mech.* **5**, 151–163.

Morton, B. R. 1962 Coaxial turbulent jets. *Intl J. Heat Mass Transfer* **5**, 955–965.

Morton, B. R., Taylor, G. I. & Turner, J. S. 1956 Turbulent gravitational convection from maintained and instantaneous sources. *Proc. R. Soc. Lond.* A **234**, 1–23.

Rodi, W. 1982 *Turbulent Buoyant Jets and Plumes.* Pergamon.

Seban, R. A., Behnia, M. M. & Abreu, K. E. 1978 Temperatures in a heated jet discharged downward. *Intl J. Heat Mass Transfer* **21**, 1453–1458.

Turner, J. S. 1966 Jets and plumes with negative or reversing buoyancy. *J. Fluid Mech.* **26**, 779–792.

Turner, J. S. 1973 *Buoyancy Effects in Fluids.* Cambridge University Press.

Turner, J. S. 1986 Turbulent entrainment: the development of the entrainment assumption and its application to geophysical flows. *J. Fluid Mech.* **173**, 431–471.

Turner, J. S. & Campbell, I. H. 1986 Convection and mixing in magma chambers. *Earth Sci. Rev.* **23**, 255–352.